13

Method of methane detection by a fiber-optic sensor using a photocatalytic nanocomposite $ZnO-SnO_2-Fe_2O_3$

© L.L. Khomutinnikova[1], I.K. Meshkovskii[1], S.K. Evstropiev[1,2,3], M.Yu. Litvinov[1], E.P. Bykov[1], S.A. Plyastsov[1]

[1] ITMO University, St. Petersburg, Russia
[2] St. Petersburg State Technological Institute (Technical University), St. Petersburg, Russia
[3] NPO „Vavilov State Optical Institute“,
192171 St. Petersburg, Russia

e-mail: larahlesnyh@yandex.ru

Received January 12, 2023
Revised January 12, 2023
Accepted February 17, 2023

The possibility of detection of methane using fiber−optical sensor with ZnO-SnO_2-Fe_2O_3C photocatalyst was demonstrated. Photocatalytic composite sensor element was prepared by non-isothermal polymer−salt method from solutions of inorganic metal salts and polyvinylpyrrolidone. Optical detection is carrying out by Bragg diffraction grating of fiber−optical sensor at the temperature variations during photocatalytic methane oxidation.

Keywords: methane, sensor, photocatalysis, fiber-optic sensor.

DOI: 10.61011/EOS.2023.03.56193.4525-23

1. Introduction

The detection of combustible gases is an important and urgent problem at all stages of their production, transport and use. Numerous research and development efforts [1–10] have been devoted to solving this problem.

Methane — the main component of natural gas — is volatile and explosive, at concentrations of 4−5% in the air it can form explosive mixtures jcite10. Therefore, the optical detection of methane in gas pipelines, oil refineries and coal fields is of particular relevance.

Currently, there are sensors based on both thermal and photocatalytic methane oxidation. For example, a Pd/Al_2O_3 based methane sensor, which was applied to Pt coils, is presented in paper [1]. Methane detection was carried out by measuring the change in sensor resistance at a temperature of 450°C, which is characterized by thermal oxidation of methane and a corresponding increase in detector circuit resistance. A $Ni_2O_3-SnO_2$ based sensor has been described in paper [2], in which the gas sensing properties were measured at a temperature of 300 − 500°C. A methane sensor based on two-dimensional ZnO nano-walls, in which the gas-sensitive properties reached their maximum values at a temperature of 300°C, was presented in [3]. The problem with existing thermal oxidation methane detectors is the high operating temperature (up to 500° C), which causes a risk of gas explosion when detecting.

The modification of metal oxide surfaces with noble metals, which can lower the detection operating temperature, is used to increase the sensitivity of methane sensors [4–8]. The $Pt/Co_3O_4/MoS_2$ based methane sensor is presented in [4], which is capable of operating at 170°C temperature. A SnO_2/Pd film sensor with sensitivity to methane at a temperature of 160°C is presented in the [5]. A methane sensor based on VO_2/Au nano-plates operating at room temperature has been developed in [6].

The development of photocatalytic gas sensors has been described in papers [8–11]. A photo-oxidative methane sensor based on hybrid graphene and ZnO/Pd structures with high sensitivity to visible light irradiation at 470 nm wavelengths has been reported in [8] . Paper [9] presents a Au-ZnO based sensor for NO detection operating at room temperature and a wavelength of 300−350 nm. The ZnO nano-fibre gas sensor proposed in paper [10] showed high sensitivity, reversible response and good selectivity for HCHO when exposed to 365 wavelength UV light at room temperature. A SnO_2/Pd based sensor, which has demonstrated high sensitivity to NO_2 when exposed to 365 wavelength UV light, has been developed at [11]. The photocatalytic composites used in [8,9,11] contain noble metals, and the problem of using more affordable components to create efficient photocatalysts is relevant.

One of the most effective photocatalysts is zinc oxide and materials based on zinc oxide [8–10,12–16]. The zinc oxide surface is sensitive to the chemical composition of the surroundings, and this material is widely used in various gas sensors (e.g., [8–10,12,13]). In [9,10], gas detection is carried out in a visible [12] or ultraviolet [10,11] (UV) light irradiation of the ZnO. Studies carried out in [14–17], have shown that the morphology and presence of structural defects in ZnO play an important role in its sensitivity to environmental changes and the spectral composition of the radiation used for photo-excitation of this material.

The purpose of this paper was to investigate the possibility of remote optical methane detection based on its photocatalytic decomposition using modern – fiber optic sensors that allow remote control of an object.

Chemical composition of the solution used and the resulting oxide composite

Composition of the film-forming solution						Composite composition, mol.%		
H_2O	Propanol-2	$Zn(NO_3)_2$	$SnCl_2$	$FeCl_3$	PVP	ZnO	SnO_2	Fe_2O_3
47.62	47.62	2.26	0.07	0.05	2.38	95	3	2

A highly dispersed nanocomposite of $ZnO-SnO_2-Fe_2O_3$ system was used as the basic photocatalytic component, whose properties have been previously described in [14]. It exhibits high photocatalytic properties under the influence of visible spectrum radiation, as well as thermal stability and chemical stability of this oxide material.

2. Materials and methods

2.1. $ZnO-SnO_2-Fe_2O_3$ photocatalyst synthesis and research methods

In this paper, $ZnO-SnO_2-Fe_2O_3$ oxide powders were produced by using a polymer – salt method according to paper [14]. Aqueous solutions of 0.26 M $Zn(NO_3)_2$, 0.26 M $SnCl_2$, 0.31 M $FeCl_3$, as well as polyvinyl pyrrolidone solution $C = 5$ wt. % (PVP) ($Mw = 10000$; BioChimica) in propanol –2. The salts and PVP solutions were mixed at room temperature and stirred continuously with a magnetic stirrer. The obtained solutions were dried at 80°C for 5 h, then the dried composite film was calcined at 550°C for 2 h to obtain composite photocatalyst powder. The composition of the solution used is shown in the Table.

The ability of the synthesized material to photogenerate chemically active singlet oxygen was investigated by luminescence spectroscopy [18] using the setup described in detail in [19].

The surface morphology of the synthesized powders was examined with a VEGA3 TESCAN scanning election microscope (SEM), at 30 kV. The crystalline phase composition was studied using a Rigaku Ultima IV X-ray diffractometer (Japan). Copper anode with $\lambda_{(CuK\alpha)} = 1.5418$ Åradiation was used. Goniometer radius 285 mm. The radiographs were taken in the range of angles $2\theta/\theta$ from 20° to 120° in the Bregg – Brentano shooting geometry. Measurements were taken using an CuK_β filter. In the experiment, the tube voltage was 40 kV, the current was 40 mA, and the output power was 1.6 kW. The scanning speed by 2θ was 5°/min. The ICDD PDF–2 (2008) diffraction database was used to interpret the diffraction reflexes.

To evaluate the photocatalytic properties of the obtained powder $ZnO-SnO_2-Fe_2O_3$, their influence on the photolysis kinetics of Rhodamine 6G (BVDA, Holland) dye in aqueous solution was studied by the methodology described in [14]. In the present paper, an aqueous dye solution ($5\cdot10^{-6}$ M) was used, made by dissolving a sample of material in distilled water. The FC solution with dye was poured into a quartz cuvette and subjected to UV irradiation using a DKBU–9 UV lamp. The kinetics of the dye decomposition process was investigated by periodically measuring the spectral properties of the irradiated dye solution. A spectrofluorimeter „Fluorat–02–Panorama" was used to measure the photoluminescence spectra in the near UV and visible spectral bands.

2.2. Methane detection experiments

Fig. 1 shows the setup for the methane photocatalytic detection experiments. According to this diagram, a cylinder of methane ($P = 150$ atm) is connected through a reducer to a closed glass tube of a total volume of 3 ml. A fiber Bragg lattice (BBL) coated with solder containing 63% Sn and 37% Pb was placed inside the glass tube. The BBL was recorded in single-mode optical fiber SMF–28 by the method [20,21]. The recorded BBL has the following characteristics: lattice length 1 mm, central wavelength 1550.392 nm, temperature sensitivity of the lattice with solder 37.52 pm/°C. The optical radiation generated by the Thorlabs S5FC1005S broadband source (BFS) was propagated along the optical fiber (OB) and fed to the BBL via a Y– Tap, after which the reflected signal was recorded by an Anritsu MS9740B optical spectroanalyzer (OSA). The thermal effect of methane photo-oxidation was detected by measuring the shift of the BBL resonance wavelength ($\Delta\lambda_B$) relative to the reference lattice, followed by converting the $\Delta\lambda_B$ values to temperature values according to the equation

$$\Delta T = \frac{\Delta\lambda_B}{K_T}, \quad (1)$$

where K_T — the temperature sensitivity of the BBL used.

For methane photocatalytic detection experiments, 0.05g of photocatalyst powder (PC) and 0.5ml of distilled water were placed in a glass tube so that the lattice was immersed in the mixture. After the mixture was incubated for 10–15 min, methane was pumped into the tube ($P = 1.5$ atm) and then the mixture was irradiated with UV light from DKBU lamp –9 (power 9 W, spectral range 205 to 315 nm, $\lambda_{max} = 254$ nm) for the set time. The wavelength change of the methane photooxidation input $\Delta\lambda_{pc}$ was measured every 30 s. The wavelength change of the reference lattice $\Delta\lambda_{\text{nn}}$ under UV irradiation was measured in parallel with this.

Under UV irradiation, the change in DVO reflects the overall temperature change of the ΔT photocatalytic cell and is determined by the combined effect of two factors: 1) heat release arising from exothermic methane photocatalytic oxidation ΔT_{pc};
2) heating of the photocatalytic cell elements by UV radiation ΔT_{uv}.

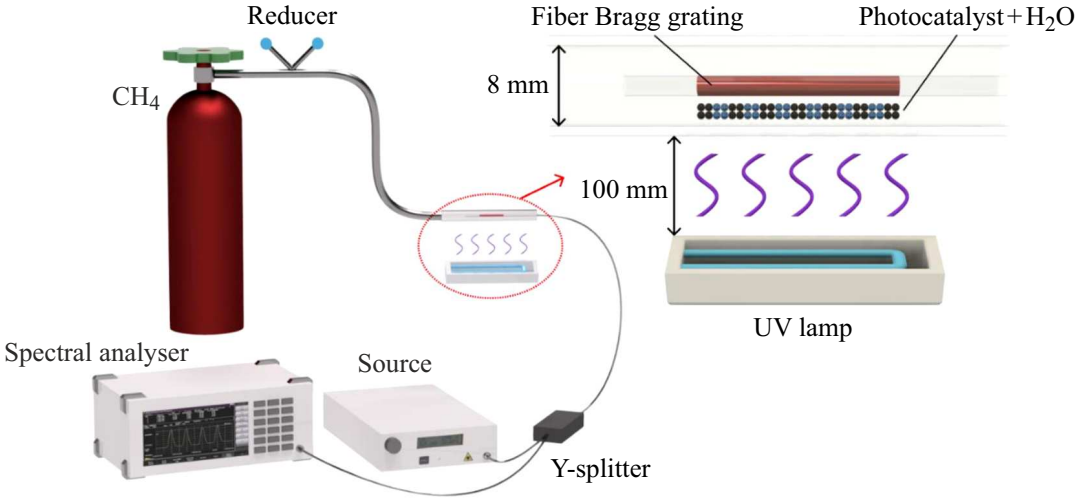

Figure 1. Schematic of an experimental setup for photocatalytic methane detection.

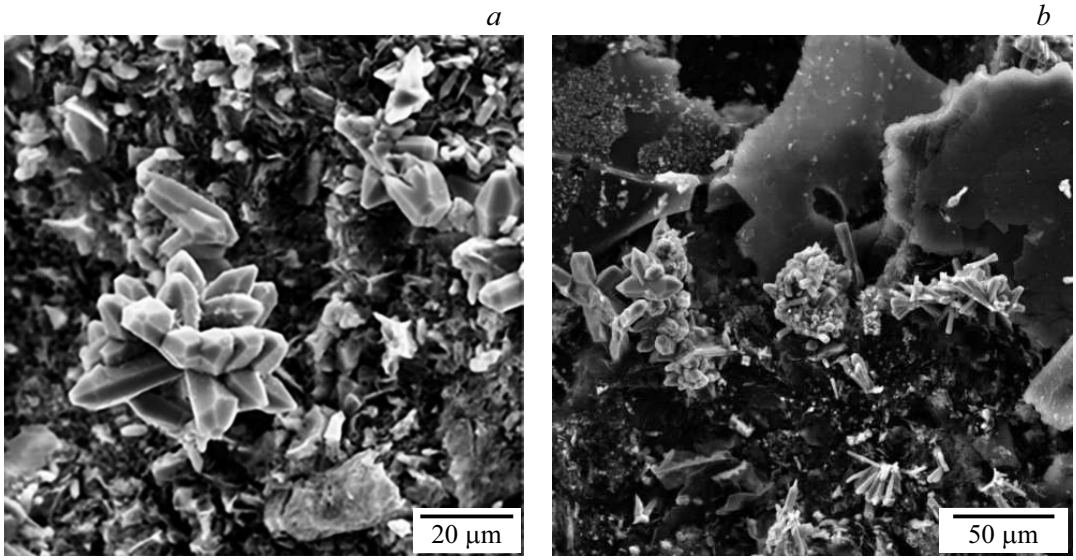

Figure 2. Electron microscopic images of photocatalytic powder ZnO 95 mol.%; SnO_2 3 mol.%; Fe_2O_3 2 mol.%.

Accordingly, the experimentally measured temperature change ΔT is:

$$\Delta T = \Delta T_{pc} + \Delta T_{uv}. \quad (2)$$

Experiments were carried out to study the effect of heating of a cell without FC under UV irradiation (corresponding to ΔT_{uv}), which allowed the influence of photocatalytic methane oxidation on cell temperature changes, i.e. ΔT_{pc}, to be determined. Given that this value is determined by the thermal effect of the exothermic reaction of methane oxidation, at the fixed parameters of the photocatalytic cell and the excitation radiation used, the value of ΔT_{pc} reflects the methane concentration in the gas mixture.

3. Results and discussions

Fig. 2 shows electronically – microscopic images of the synthesized photocatalytic powder with its chemical composition: ZnO 95 mol. %; SnO_2 3 mol. %; Fe_2O_3 2 mol. %. The illustration shows that the powder consists of particles and aggregates and also contains microcrystalline formations having the form „colors“, containing hexagonal zinc oxide microcrystals. This powder morphology is due to the non-simultaneous crystallization of different oxides in the non-isothermal heat treatment process of the initial mixture and ensures high photocatalytic characteristics of the material [14].

X-ray diffraction analysis of the synthesized powder showed the presence of hexagonal zinc oxide crystals (JCPDS 01–070–8072). Calculations using the Scherrer

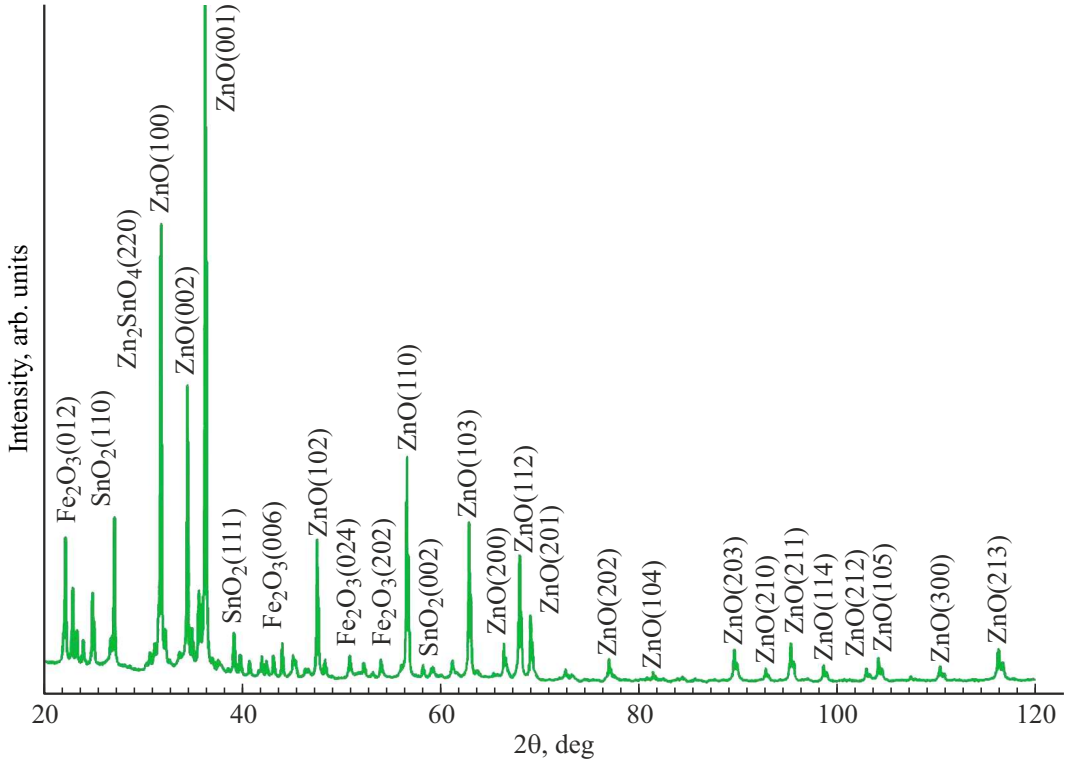

Figure 3. X-ray of photocatalytic powder ZnO 95 mol.%; SnO_2 3 mol.%; Fe_2O_3 2 mol.%.

formula showed that the average size of the zinc oxide crystals in the samples is $46 \div 49$ nm. The presence of SnO_2 and Fe_2O_3 in the photocatalyst composition leads to the appearance of these oxides as well as cubic crystals of zinc orthostannates and ferrites ($ZnSnO_4$ (JCPDS 24−1470) and $ZnFe_2O_4$ (JCPDS 79−1150)) on X-ray patterns (Fig. 3). These crystals, like zinc oxide, have photocatalytic properties, which can generate reactive oxygen intermediates [22,23] and oxidize methane.

Fig. 4 shows the photoluminescence spectrum ($\lambda_{ex} = 405$ nm) of the oxide powder in the near infra-red (IR) area of the spectrum. In the spectrum, an emission band with a maximum of 1270 nm, characteristic of chemically active singlet oxygen and corresponding to the electronic transition $^1\Delta_g - ^3\Sigma_g$ [18], is observed. It should be noted that photogeneration of reactive oxygen is observed under the influence of radiation in the visible spectral range.

The Langmuir-Hinshelwood [24,25] model is often used to describe the kinetics of photocatalytic decomposition of dyes in solutions. According to this model, the change in concentration of C dye in dilute ($C \ll 10^{-3}$ M) solutions is described by a pseudo-first order photocatalytic rate equation.

$$\frac{C}{C_0} = e^{-kt}, \qquad (1)$$

where C_0 — the initial dye concentration in solution, k — the first order rate constant of pseudo −.

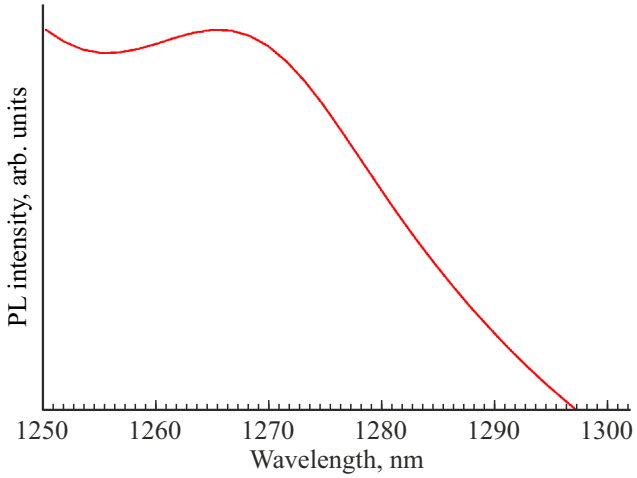

Figure 4. Photoluminescence spectrum ($\lambda_{exc} = 405$ nm) of photocatalytic powder ZnO 95 mol.%; SnO_2 3 mol.%; Fe_2O_3 2 mol.%.

Fig. 5 illustrates the effect of photocatalyst addition on the photodegradation kinetics of Rhodamine 6G dye in aqueous solution. It should be noted that in the absence of photocatalyst additions, the dye photodegradation in solution was 20 times slower.

Fig. 6 shows the average of four independent experiments as a function of the change in the DVO ($\Delta\lambda$) of photocatalyst-loaded BBL (curve *1*) and control BBL

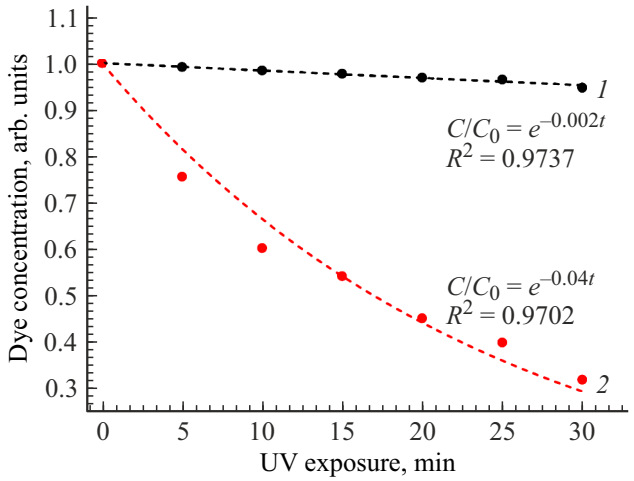

Figure 5. Effect of the duration of UV irradiation on the change in relative dye concentration in aqueous solution (curve *1*) and in analogous solution containing photocatalytic powder (curve *2*).

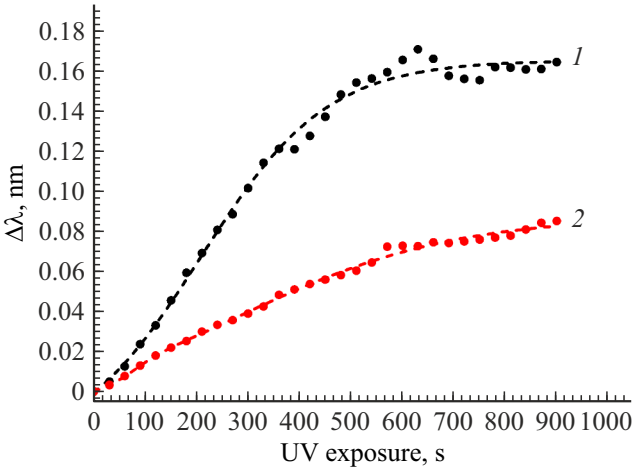

Figure 6. Kinetics of wavelength changes of reflectance of photocatalyzed BBL (curve *1*) and control BBL (curve *2*) in the photocatalytic methane oxidation process.

without photocatalyst (curve *2*) depending on the duration of UV exposure to PC in a methane-water environment. The Fig. also shows that at irradiation duration of 800 s the BBL DVO with photocatalyst (curve *1*) ceases to change, which is due to complete conversion of methane during its oxidation and the corresponding cessation of heat release.

Fig. 7 shows the kinetic dependence of the temperature change ΔT_{pc} in the cell, determined by heat release in the methane photocatalytic oxidation process, averaged from four independent experiments. From the kinetic curve, it can be seen that the methane photo-oxidation reaction can be divided into three periods: I— induction period from 0 to 125.s; II— rate increase period from 125 to 289.s; III— rate slowing period over 289 s.

Furthermore, the derivative curve of ΔT_{pc} shows that the maximum rate of the photo-oxidation process is observed at 207 s and is 7.51 mK/s. Thus, the most effective methane

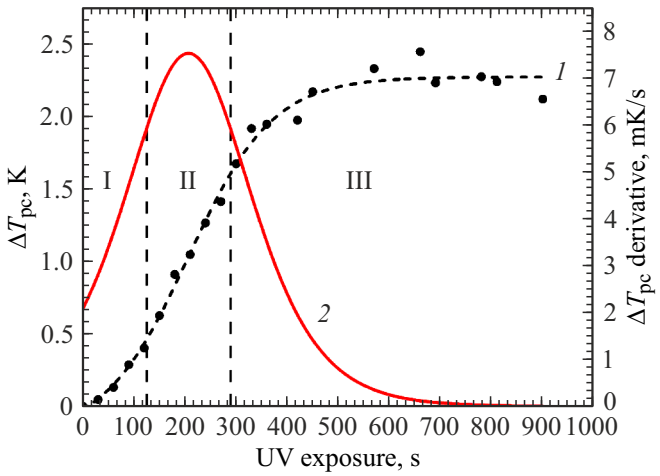

Figure 7. Kinetics of temperature change in the process of photocatalytic oxidation of methane (*1*) and its derivative (*2*).

photooxidation is observed in the 125 to 289 s region, with maximum ΔT_{pc} values obtained in the experiments on this time region, reaching ~ 3 K.

Conclusions

The paper demonstrates the possibility of optical methane detection by an – fiber optical sensor using ZnO–SnO$_2$–Fe$_2$O$_3$ photocatalytic nanocomposite. The nanocomposite was synthesized by the – polymer-salt method, consisted of a mixture of different oxide crystals smaller than 50 nm and was characterized by its ability to photogenerate chemically reactive oxygen intermediates and photocatalytic activity. Optical methane detection was carried out by registering temperature changes caused by methane oxidation in a photocatalytic cell using a temperature-sensitive fiber-optic sensor. The maximum rate of photo-oxidation was observed at 207 s and was 7.51 mK/s.

Conflict of interest

The authors declare that they have no conflict of interest.

References

[1] F. Liu, Y. Zhang, Y. Yu, J. Xu, J. Sun, G. Lu. Sensors and Actuators B: Chemical, **160** (1), 1091-1097 (2001)

[2] Nguen Minh Vuong, Nguen Minh Hieu, Hoang Nhat Hieu, Hwangpyo Yi, Dojin Kim, Yong-Shik Han, Myungbae Kim. Sensors and Actuators B: Chemical, **192**, 327-333 (2014). DOI: 10.1016/j.sub.2013.10.117

[3] T.-P. Chen, S.-P. Chang, F.-Y. Hung, S.-J. Chang, Z.-S. Hu, K.-J. Chen. Sensors, **13**, 3941-3950 (2013). DOI: 10.3390/s130303941

[4] D. Zhang, H. Chang, Y. Sun, C. Jiang, Y. Yao, Y. Zhang. Sensors and Actuators B: Chemical, **252**, 624-632 (2017). DOI: 10.1016/j.sub.2017.06.063

[5] D. Haridas, V. Gupta. Chemical, **166-167**, 156-164 (2012). DOI: 10.1016/j.sub.2012.02.026
[6] J. Liang, W. Li, J. Liu, M. Hu. Mater. Lett., **184**, 92-95 (2016). DOI: 10.1016/j.matlet.2016.08.030
[7] Z.P. Tshabalala, K. Shingange, B.P. Dhonge, O.M. Ntwaeaborwe, G.H. Mhlongo, D.E. Motaung. Sensors and Actuators B: Chemical, **238**, 402-419 (2017). DOI: 10.1016/j.sub.2016.07.023
[8] Y. Xia, J. Wang, L. Xu, X. Li. S, Sensors and Actuators B: Chemical, **304**, 127334 (2020). DOI: 10.1016/j.sub.2019.127334
[9] N. Gogurla, A.K. Sinha, S. Santra, S. Manna, S.K. Ray. Sci Rep, **4**, 6183 (2014). DOI: 10.1038/srep06483
[10] J. Cui, L. Shi, T. Xie, D. Wang, Y. Lin. Sensors and Actuators B: Chemical, **227**, 220-226 (2016). DOI: 10.1016/j.sub.2015.12.010
[11] F.H. Saboor, T. Ueda, K. Kamada, T. Hyodo, Y. Mortazavi, A.A. Khodadadi, Y. Shimizu. Sensors and Actuators B: Chemical, **223**, 429-439 (2016). DOI: 10.1016/j.sub.2015.09.075
[12] Q, Geng, Z. He, X. Chen, W. Dai, X. Wang. Sensors and Actuators B: Chemical, **188**, 293-297 (2013). DOI: 10.1016/j.sub.2013.07.001
[13] S. Park. Current Appl. Phys, **16** (10), 1263–1269 (2016). DOI: 10.1016/j.cap.2016.07.005
[14] L.L. Khomutinnikova, S.K. Evstropiev, D.P. Danilovich, I.K. Meshkovskii, D.V. Bulyga. J. Composite Science, **6**, 331 (2022). DOI: 10.3390/jcs6110331
[15] Md. T. Uddin, Y. Nicolas, C. Olivier, T. Toupance,L. Servant, M.M. M̈ller, H.-J. Kleebe, J. Ziegler, W. Jaegermann. Inorg. Chem., **51** (14), 7764-7773 (2012). DOI: 10.1021/ic300794j
[16] S.K. Evstropiev, L.V. Lesnykh, A.V. Karavaeva, N.V. Nikonorov, K.V. Oreshkina, L.Yu. Mironov, S.Yu. Maslennikov, E.V. Kolobkova, I.V. Bagrov. Process Intensification, **142**, 107587, (2019). DOI: 10.1016/j.cep.2019.107587
[17] D.V. Bulyga, S.K. Evstropiev. Opt. i spektr., **130** (9), 1455-1463 (2022). (in Russian). DOI: 10.21883/OS.2022.09.53309.3617-22
[18] D. Toshiro, N. Yoshio. J. Phys. Chem., **111**, 4420–4424 (2007).
[19] V.M. Kiselev, I.M. Kislyakov, A.N. Burchinov. Opt. Spectrosc, **120** (4), 520-524 (2016).
[20] A.I. Gribaev, S.V. Vargel, K.A. Connov, A.M. Stam, R.F. Idrisov, Y.I. Slozhenikina. Izv. vuzov. Priborostroenie. **60** (5), 466-473 (2017) (in Russian). DOI: 10.17586/0021-3454-2017-60-5-466-473
[21] K.A. Connov, E.A. Frolov, A.I. Gribaev, V.V. Zakharov, A.A. Mikhneva, V.A. Novikova, S.V. Vargel. Opt. i spektr., **125** (1), 51-56 (2018). (in Russian). DOI: 10.21883/OS.2018.07.46266.2-18
[22] X. Lou, X. Jia, J. Xu, S. Lin, Q. Gao. Mater. Sci. Engineering: A, **432** (1-2), 221-225 (2006).
[23] S. Song, X. Yang, Y. Zhang, F. Zhang, J. Ding, J. Bao, C. Gao. Progress in Natural Sci.: Mater. Int., **22** (6), 639-643 (2012). DOI: 10.1016/j.pnsc.2012.11.008
[24] V.I. Gaya, A.H. Abdullah. J. Photochem. Photobiol. C: Photochem., **9**, 1-12 (2008). DOI: 10.1016/j.jphotochemrev.2007.12.003
[25] I.K. Konstantinou, T.A. Albanis. Appl. Catalysis B: Environmental, **49** (1), 1-14 (2003). DOI: 10.1016/j.apcatb.2003.11.010

Translated by Ego Translating